JOURNAL OF MATERIALS SCIENCE **35** (2000) 3347–3357

Video-controlled tensile testing of alumina fibres and rods manufactured by colloidal processing

D. COIMBRA*, R. GREENWOOD, K. KENDALL
Birchall Centre for Inorganic Chemistry and Materials Science, School of Chemistry and Physics, Keele University, Keele, Staffs, ST5 5BG, UK
E-mail: chd73@keele.ac.uk

Concentrated suspensions of alumina were prepared from a commercially available raw powder stabilised with a dispersant. These suspensions were then mixed with a fixed amount of binder and milled for different times, resulting in distinct particle size distributions. The stabilised slurries were tape-cast and dried in an oven at constant temperature and humidity. Good aggregate free pastes were generated from this colloidal process. The pastes were then extruded through various sized dies (from 300 μm to 1.6 mm in diameter), to form fibres and rods of different diameters. These were finally sintered in air at different temperatures: 1400°C, 1500°C and 1600°C. The mechanical properties of these single strand alumina fibres, i.e. Young's modulus and tensile strength, were determined using a computer-assisted video extensometer. The effects of powder processing, sample diameter and sintering temperature on the tensile properties were therefore investigated.

1. Introduction

The potential benefits of colloidal processing to give high-strength sintered ceramics have been recognised for a long time [1–3]. It is known through the Griffith equation (1) that the strength of ceramic materials is limited by the flaw size of the body [4]:

$$\sigma_f = \frac{K_{IC}}{Y\sqrt{c}} \quad (1)$$

where σ_f is the strength, K_{IC} the fracture toughness, Y a geometrical factor and c the flaw size. Hence for strong ceramics it is important to minimise the size of the flaws. These flaws are directly attributable to aggregates in the initial ceramic powder, formed by the ubiquitous van der Waals attractive force, which causes submicron size particles to stick together. However, colloidal processing allows these aggregates to be destroyed, hence reducing the size of the flaws to that of the particle size [5]. With no or minimal flaws present, the sintered body is stronger and more reliable. Hence, the first part of any investigation into the production of ceramic pastes (e.g. for extrusion) must address the issue of how to adjust the interparticle forces.

In colloid science, there are classically two ways to prevent particles aggregating [6]. The first is to introduce charges to the surface such that the particles repel one another through simple electrostatic repulsion. The second method is to adsorb polymers onto the particle surface such that the particles cannot physically come close enough for the van der Waals attraction to dominate. This is termed steric stabilisation.

Traditionally in the ceramic industry, particle stability is obtained by the adsorption of polyelectrolyte dispersants onto the ceramic powder surface. These impart stability to the particles by a combination of electrostatic and steric effects—or "electrosteric" for short. It is important to select the correct dispersant and add the correct amount to avoid flocculation. This optimum amount may be located by adsorption isotherms, rheology, electrophoresis or acoustophoresis [7, 8]. Acoustophoresis has the advantage of working on concentrated ceramic suspensions compared to the diluted suspensions required for electrophoresis. Once a suitable dispersant is located for the powder, it is then necessary to produce a concentrated suspension. This is normally obtained by wet-milling the powder in the presence of the dispersant to break down the aggregates and expose new surfaces for its adsorption. In order to convert the concentrated suspension into a paste, it is necessary to dry it. However, prior to this, a binder is added into the slurry to confer some strength to the body for ease of handling once dry. The suspension is then tape-cast to form a thin sheet and the solvent used during the milling step evaporates off to leave a paste. The pastes produced in this study were collected into a barrel and extruded at room temperature. These were then sintered in air and tested with a video extensometer. The potentialities of this system to record very low strain levels have been shown in a previous paper [9].

The effect of milling time during the slurry preparation, after addition of binder, has been studied and two suspensions having different particle size distributions

* Author to whom all correspondence should be addressed.

were characterised. The mechanical properties after sintering, i.e. Young's modulus and tensile strength, could then be directly related to the dispersion state of the powder: coarse (characteristic of remaining aggregates after milling) and fine (typical of a well-dispersed suspension). These two suspensions were made into pastes and extruded through different sized dies to make fibres or rods of varying size ranges. For the purpose of this paper, the articles produced below 1 mm in diameter are termed "fibres" whilst the rest are termed "rods". Because of their larger diameter, rods should, on average, have a greater chance of having large flaws and would therefore be weaker than fibres. The Griffith equation (1) was used to calculate the flaw size relatively to the specimen diameter. Three sintering temperatures were employed to study the effect of densification on the mechanical properties: 1400°C, 1500°C and 1600°C. This wide range allowed fabrication of fibres and rods having different porosity levels.

Mechanical properties of ceramic materials, including elastic moduli and tensile strength, decrease with increasing porosity [10]. The effect of porosity on the Young's modulus of the colloidally made alumina fibres will be discussed and experimental results will be fitted using a simple empirical equation. The effect of grain size on tensile strength has been surveyed in the past [11] and will also be discussed in the present study. Microstructural analysis was carried out to bring in complementary information.

2. Experimental section

Concentrated suspensions of alumina in double distilled water were prepared by stabilising the raw powder (SDK A160 SG1, Showa Denko's c/o Whitfield & Son Ltd, UK) with a dispersant. The powder has been characterised by X-Ray fluorescence spectroscopy (PW1606, Phillips, Netherlands) for elemental composition and BET nitrogen adsorption (Gemini 2360, Micromeritics, USA) for specific surface area. The best dispersant and its optimum amount have been investigated by acoustophoresis in a previous study [12].

The powder and dispersant were vibro-energy milled (Grinding mill, Sweco, Belgium), for 45 minutes, in 1 L poly(ethylene) bottles containing double distilled water (conductivity $<0.5\ \mu S \cdot cm^{-1}$). The quantities of all the raw materials used to prepare the slurries are listed in Table I. The mass of zirconia grinding media (beads having approximately 1 cm in size) was approximately 2.3 times that of the powder. The dispersion of the suspension was then characterised by measuring the particle size distribution (Mastersizer E, Malvern Instruments Ltd, UK). A unimodal distribution indicated a good dispersion state whilst a multimodal distribution indicated a poor dispersion. A fixed amount of Poly(vinyl alcohol) (Gohsenol KH17S, Nippon Gohsei, Japan) in water (0.14 g/g) was then added to the suspension. This binder was added to confer some strength to the body for ease of handling once dry. The suspension was then vibro-energy milled longer, in the presence of binder, additional water and a small amount of plasticiser (Table I). The preparation of the slurry could then be divided in two main stages: dispersion and homogenisation. The effect of vibro-energy milling time during the second stage was characterised by measuring the particle size distribution at different intervals over 200 hours.

TABLE I Preparation conditions of the alumina suspensions

Compound	Nature	Amount (g)	Milling time (h)
Powder	SDK A160 SG1	475	
Dispersant	Dispex A40	2.78	0.75
Solvent	Distilled water	100	
Grinding media	Zirconia beads	1100	
Binder	PVA in water (0.14 g/g)	254.3 (35.6 active)	
Plasticiser	1-Octanol	31.66	Variable
Solvent	Distilled water	180	

The suspensions were tape-cast onto acetate supports attached to smooth glass plates to form 180 μm thick sheets. The plates were placed in a constant humidity cabinet (Fisons, UK) to ensure a fast and uniform drying of the tapes. Pastes could be obtained after approximately 10 minutes by keeping a dry temperature of 50°C and a relative humidity of 21%. The pastes were then rolled into balls and mixed by hand to have a good homogeneity, before being placed inside the barrel of an extruder. A universal testing machine (6000R, Lloyds Instruments Ltd, UK) was used to extrude the pastes through 300, 500, 1000, 1200 and 1600 μm sized dies (British Diamond Wire, UK).

After being dried at room temperature for at least 24 hours, the extrudates were sintered in air with the final sintering dwell temperature being 1400°C, 1500°C or 1600°C. The heating rate from room temperature to 500°C was kept relatively slow (1°C/min) to avoid any failure in the final product due to a non-homogeneous burn out of the organic compounds. After 500°C, all the organic additives had burnt out and a faster heating rate could be used. In all cases, the dwell time was maintained at 1 hour.

The mechanical properties of the fibres and rods, i.e. Young's modulus and tensile strength, were finally characterised using a computer-assisted video extensometer (ME-46 Full Image Videoextensometer, Messphysik Laborgeräte GES.m.b.H., Austria). The principles of operation and settings for testing ceramic materials have been described in a previous article [9]. Ten measurements at least were performed to determine an experimental mean value corresponding to a particular diameter and sintering temperature. The specimen length ranged from 80 to 120 mm. The distance between the targets was kept greater than 40 mm (for a camera field of view of 80 mm). The universal testing machine (LRX, Lloyds Instruments Ltd, UK) was fitted with a 50 N and a 2500 N load cell, for testing fibres and rods respectively. The crosshead speed during testing was maintained at 0.2 mm/min. An optical microscope (BX 50, Olympus, Japan) working in transmission mode and fitted with a CCD colour video camera (KY-F55B, JVC, Japan) was used to accurately measure the diameter of the specimens before testing. This parameter had to be precisely determined to accurately calculate the

Young's modulus and tensile strength using the video extensometer post-processing software.

After mechanical testing, the remaining sample pieces were collected for determination of the density. Density measurements were carried out using Archimedes principle. A density bottle of 10 ml was used to weigh the samples in water on a digital precision balance (Ohaus Corp., USA). More than 2 grams were required to get reliable results for each sample. The bottle had a pierced lid so that at no point was air trapped in the water when filled. The porosity (P) could then be estimated by using the following equation:

$$P = 1 - \frac{D_{\text{exp}}}{D_{\text{th}}} \tag{2}$$

where D_{exp} is the measured density and D_{th} is the theoretical density of α-alumina ($D_{\text{th}} = 3.987$ g/cm^3).

Finally a scanning electron microscope (S-4500, Hitachi, Japan) was used to look at the microstructure of 1 mm rods produced from two suspensions having different particle size distributions and sintered at different temperatures. The average grain size was calculated using an image measurement software (Sigma Scan Pro, Jandel Scientific, USA) and taking the average of more than 200 grain sizes on the same picture.

TABLE II XRF analysis of the alumina raw powder (SDK A160 SG1)

Compound	Amount (%)
Silica (SiO_2)	<0.02
Titania (TiO_2)	<0.01
Alumina (Al_2O_3)	99.8 (By difference)
Ferric oxide (Fe_2O_3)	<0.01
Lime (CaO)	0.01
Magnesia (MgO)	0.05
Potash (K_2O)	<0.01
Soda (Na_2O)	<0.03
Loss on ignition at 1025°C	0.11

3. Results

3.1. Powder characteristics

The measured surface area of the alumina powder was 7.1 m^2/g, indicating that it was not a particularly fine powder. The elemental composition, determined by X-Ray fluorescence (XRF), is listed in Table II. The proportion of impurities was low (<0.2%) and the powder therefore had a high purity level. A low level of magnesia (0.05%) was also present, which is included as a sintering aid.

3.2. Effect of the milling time

After addition of binder, particle size distribution measurements were taken at different intervals over a long period. The evolution of the d_{10}, d_{50} and d_{90} is displayed in Fig. 1 and shows that the lowest particle size is obtained for milling times between 30 and 150 hours approximately. Between 0 and 30 hours, agglomerates induced by the polymer addition are easily crushed. The solution homogenises and the polymer bonds to the colloidal particles. Steric repulsion increases and the particle size decreases. After 30 hours, all the agglomerates have disappeared and the individual alumina crystals are dispersed. The particles are uniformly covered with binder and the particle size remains stable. After 150 hours, the high energy of milling has broken down alumina particles. However, the amount of dispersant is limited and may not be enough to cover the split particles. The polymer might then adsorb onto the uncovered surfaces and bond particles together, leading to re-agglomeration. This would explain the increase in particle size after 150 hours of milling [13].

Two suspensions having different particle size distributions were prepared. The first, termed "SDK1 (2 h)", was made by milling the suspension with binder for 2 hours and contained a significant proportion of aggregates. The second, termed "SDK2 (30 h)" was milled for 30 hours after addition of binder, and corresponded to a well de-aggregated suspension. The difference in particle size was significant (Table III) and the effect of dispersion and aggregation on mechanical properties could be further studied.

3.3. Mechanical properties

All stress-strain curves obtained in this study were linear up to the fracture stress. This linear elastic behaviour

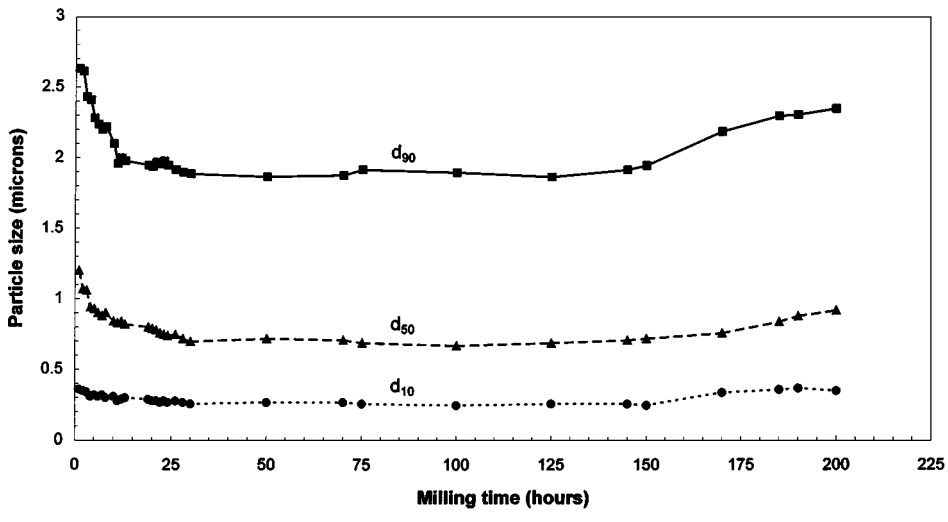

Figure 1 Evolution of the particle size distribution after addition of binder.

TABLE III Particle size distribution of the two suspensions used in this study (before extrusion)

Distribution	Particle size (SDK1 (2 h)) (μm)	Particle size (SDK2 (30 h)) (μm)
d_{10}	0.35	0.26
d_{50}	1.07	0.70
d_{90}	2.61	1.89

is typical of brittle materials, such as alumina, at room temperature [10].

3.3.1. Young's modulus

The elastic constant measurements gave different results for "SDK1 (2 h)" and "SDK2 (30 h)" but the same trends could be observed (Figs 2 and 3). In all cases, the Young's modulus did not depend on the specimen diameter and experimental results could be fitted with straight lines, as shown on the graphs. This result was expected as the Young's modulus (E) is an elastic constant which can be defined for isotropic materials as the stress required to give unit strain in the same direction, without restraint in the orthogonal directions [14].

At room temperature, this elastic property depends on the phase constitution, and the shape and distribution of any porosity, since pores act as a second phase of zero modulus. Assuming that no major contamination occurred during sintering, the samples were all considered single phased. Hence porosity was considered as the main factor which could influence the results. The denser the material, the higher the Young's modulus. Density measurements were performed for both SDK1 (2 h) and SDK2 (30 h), and results showed that porosity decreased with temperature between 1400°C and 1600°C (Figs 4 and 5). Hence the Young's modulus increased with the sintering temperature.

For alumina materials (>99% Al_2O_3), a Young's modulus of 380 GPa was taken as reference [15]. The values obtained after fitting the experimental data were different for the two suspensions studied (Table IV) and showed the influence of the particle size distribution, and consequently the role of the densification process during sintering. SEM pictures are given in Fig. 6 to compare the microstructures of SDK1 (2 h) and SDK160 (30 h) 1 mm rods between 1400°C and 1600°C. At 1400°C, pictures A and D show limited grain necking, which signifies that the densification

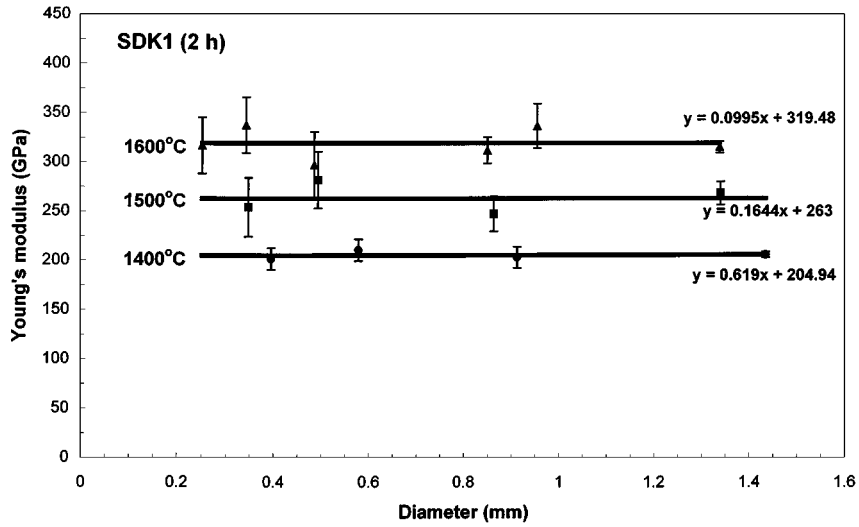

Figure 2 Elastic constant of "SDK1 (2 h)" fibres and rods sintered at different temperatures.

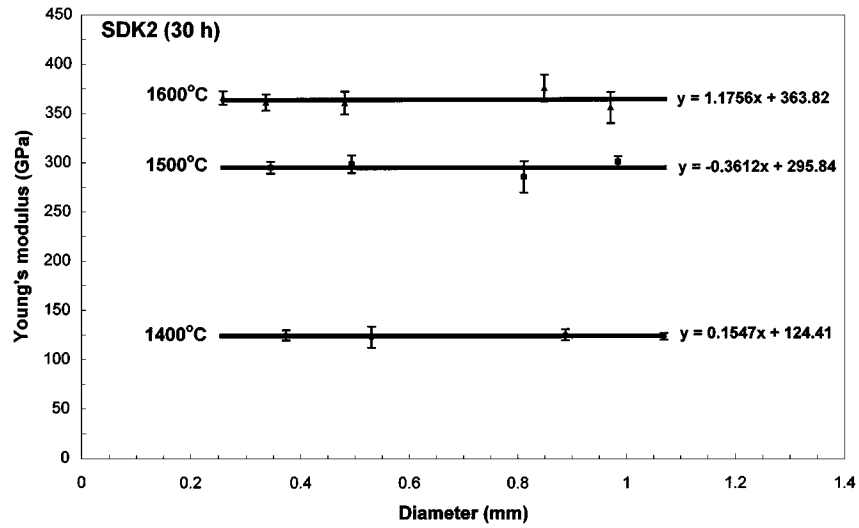

Figure 3 Elastic constant of "SDK2 (30 h)" fibres and rods sintered at different temperatures.

TABLE IV Experimental Young moduli (obtained after fitting)

Sintering temperature (°C)	E(SDK1 (2 h)) (GPa)	E(SDK2 (30 h)) (GPa)
1400	205	125
1500	263	296
1600	320	364

process has just started. The porosity is large and the numerous small particles indicate that the grain growth has not initiated. Many aggregates can be seen on picture A (SDK1 (2 h)) and confirm the particle size distribution analysis. A much finer and homogeneous microstructure can be seen on picture D, resulting in a very high porosity and a significantly lower Young's modulus. At 1500°C, grains have started to grow and fewer pores are present. Large aggregates are still observed for SDK1 (2 h) (picture B). SDK2 (30 h) is not fully densified at 1500°C (picture E) but the microstructure appears much more homogeneous, hence resulting in a lower porosity and a greater Young's modulus. At 1600°C, the same conclusions can be drawn whilst the structures have fully densified and grains have significantly grown. Therefore, the influence of porosity on elastic constants could be qualitatively interpreted by a microstructure analysis. A fine and homogeneous microstructure is necessary to achieve an optimum densification and obtain a high Young's modulus close to the target value of 380 GPa. Values of 364 GPa and 320 GPa were obtained for SDK2 (30 h) and SDK1 (2 h), respectively, at 1600°C. A discrepancy of 44 GPa was therefore measured, using the sane experimental conditions, and this could be directly related to the presence of aggregates in the initial composition.

3.3.2. Tensile strength

Similar trends were observed for SDK1 (2 h) and SDK2 (30 h) when considering the effect of specimen diameter on the strength (Figs 7 and 8). At any one sintering temperature, the larger the diameter, the lower the strength. This result is expected, as it is more likely to find larger strength-limiting defects in greater volumes. The fitting of the experimental curves could be reasonably assimilated to a square root power law dependence. This would indicate that the higher shear stress in the smaller dies is breaking the larger agglomerates.

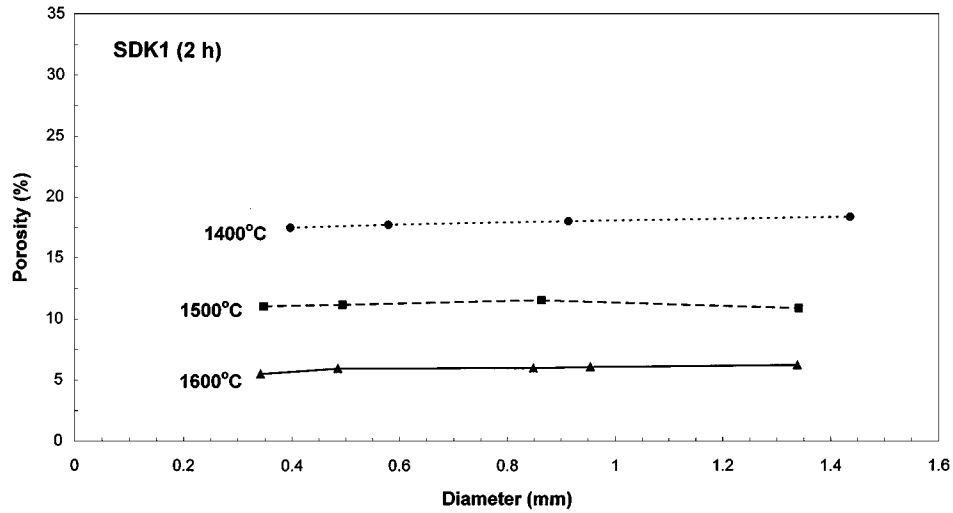

Figure 4 Porosity of SDK1 (2 h) fibres and rods sintered at different temperatures.

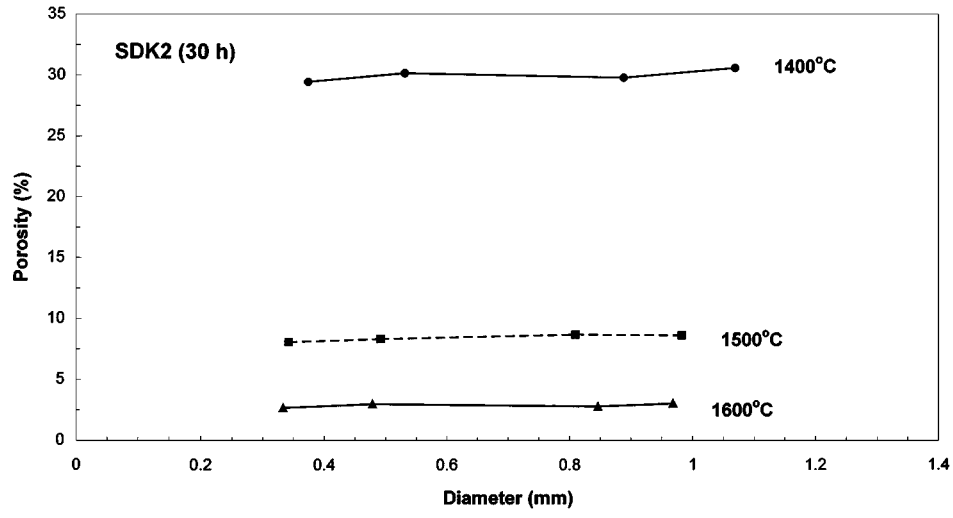

Figure 5 Porosity of SDK2 (30 h) fibres and rods sintered at different temperatures.

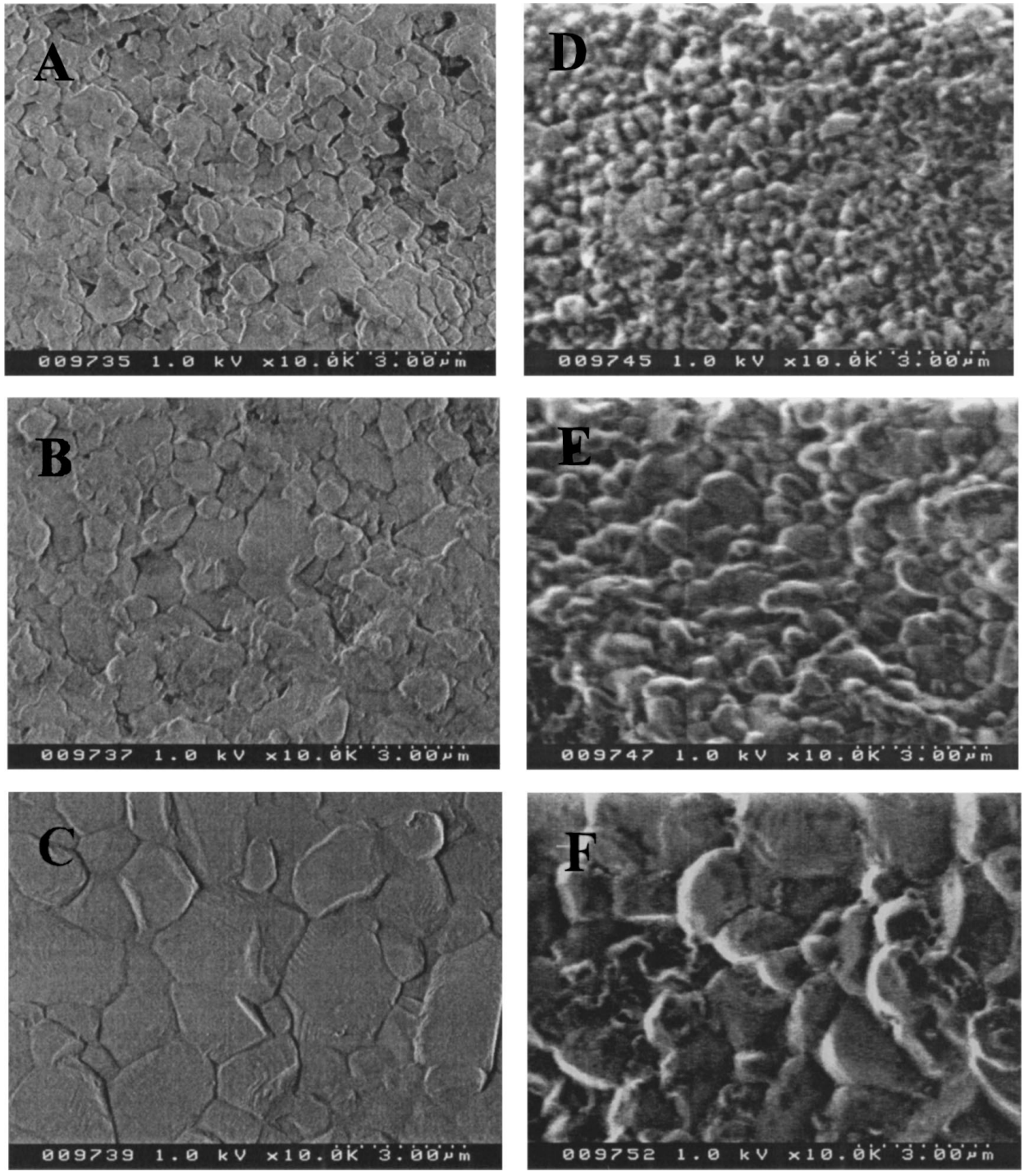

Figure 6 SEM pictures of 1 mm rods—SDK1 (2 h) sintered at 1400°C (A), 1500°C (B), 1600°C (C) and SDK2 (30 h) sintered at 1400°C (D), 1500°C (E), 1600°C (F).

The breaking stress of a ceramic material depends on these main factors:

– The shape, size, position and orientation of strength-limiting defects. This includes internal defects, such as pores, contaminants, cracks, exaggerated grain growth, etc; and surface defects, like debris, dirt, impacts, etc.

– The fracture toughness (K_{IC}) of the material. For alumina, a value of 4 MPa $\cdot$ $m^{1/2}$ is commonly used.

– The stiffness of the material, i.e. Young's modulus.

Aggregates are likely to create flaws in sintered bodies, such as pores and exaggerated grain growth, leading to a significant drop in strength. This was confirmed by comparing the experimental results obtained at 1500°C and 1600°C: SDK2 (30 h) was stronger than SDK1 (2 h). At 1400°C, the situation was reversed because SDK2 (30 h) was much more porous than SDK1 (2 h), as shown in Figs 4 and 5.

The strength varied with the sintering temperature and, again the behaviour could be directly related to the presence of aggregates in the initial composition. Maximum strengths were achieved at 1500°C in both cases. This corresponded to a good densification process, without creation of important limiting-strength defects by grain growth. At 1600°C, a large reduction in strength was observed for SDK1 (2 h) whilst the drop

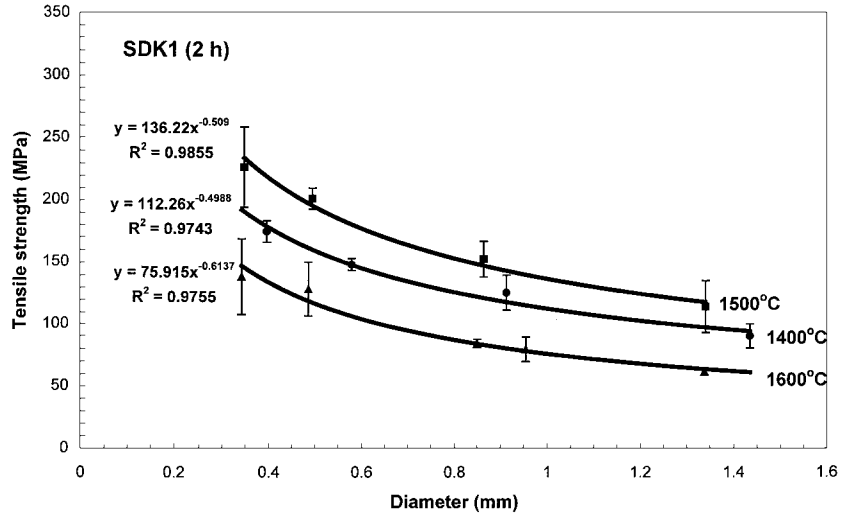

Figure 7 Tensile strength of "SDK1 (2 h)" fibres and rods sintered at different temperatures.

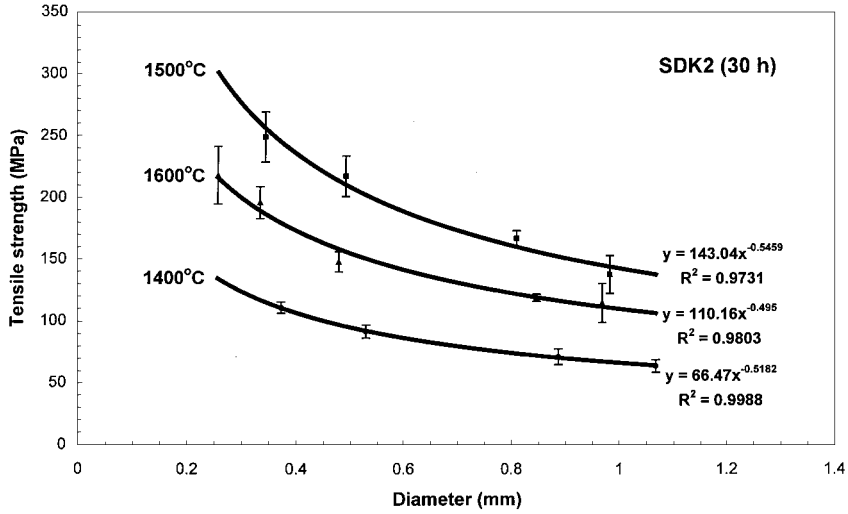

Figure 8 Tensile strength of "SDK2 (30 h)" fibres and rods sintered at different temperatures.

was limited for SDK2 (30 h). Because of the dependence of strength on grain size [11], exaggerated grain growth could then be suspected of being the dominant flaw. An image measurement software was used with SEM pictures to calculate the average grain size (for 1 mm rods only) in relation to the sintering temperature (Fig. 9). Despite a significant increase at 1600°C, the grain size was relatively small (<2 μm), and no exaggerated grain growth could be measured. However, examination of the SEM pictures showed the presence of several aggregates for SDK1 (2 h), whereas SDK2 (30 h) was free of large aggregates. At 1400°C, SDK2 (30 h) was not fully sintered and the porosity was high (approx. 30%), leading to a large reduction in strength. SDK1 (2 h) was less porous (approx. 18%) and the drop in strength was less important. The material was stronger at 1400°C than at 1600°C, indicating that the aggregates influenced the strength more than the pores, to a certain level of porosity (<20%). If the porosity was too high, then the pores dominated large aggregates as the main origin of strength-limiting flaws. No data have been found in the literature to compare with the strength values obtained in the present study. The strength of ceramic materials depends on many factors, such as the testing method and specimen specifications, and it is almost impossible to compare data from different sources. However, using the fitting equations (Figs 7 and 8), tensile strengths could be calculated for different diameters. A value greater than 1400 MPa is indicated for "Fiber FP" (Du Pont, USA) having a diameter of 20 μm [16]. Considering the best experimental results (obtained at 1500°C), values of 1000 MPa and 1200 MPa could be estimated for SDK1 (2 h) and SDK2 (30 h), respectively. The data could not be directly compared, as the testing method was different, but they fell within the same order of magnitude.

4. Discussion

4.1. Calculation of the Young's moduli

Spriggs [17] studied the effect of porosity on elastic constants and proposed the following equation:

$$E = E_0\, e^{-\mathrm{bP}} \tag{3}$$

where E is the Young's modulus of the porous polycrystalline body, E_0 is the Young's modulus the nonporous polycrystalline body, e is the Napierian number (2.71828...), b is an empirical constant, and P is the fractional pore volume of the body. Knudsen [18] studied the effect of porosity, up to 40%, on

TABLE V Comparison between experimental ("Exper.") and calculated ("Calc.") Young's moduli (obtained after fitting)

	SDK1 (2 h)			SDK2 (30 h)		
Sintering temperature (°C)	Exper. E (GPa)	Calc. E (GPa)	Deviation (%)	Exper. E (GPa)	Calc. E (GPa)	Deviation (%)
1400	205	207	0.97	125	129	3.10
1500	263	262	0.38	296	300	1.33
1600	320	330	3.03	364	368	1.08

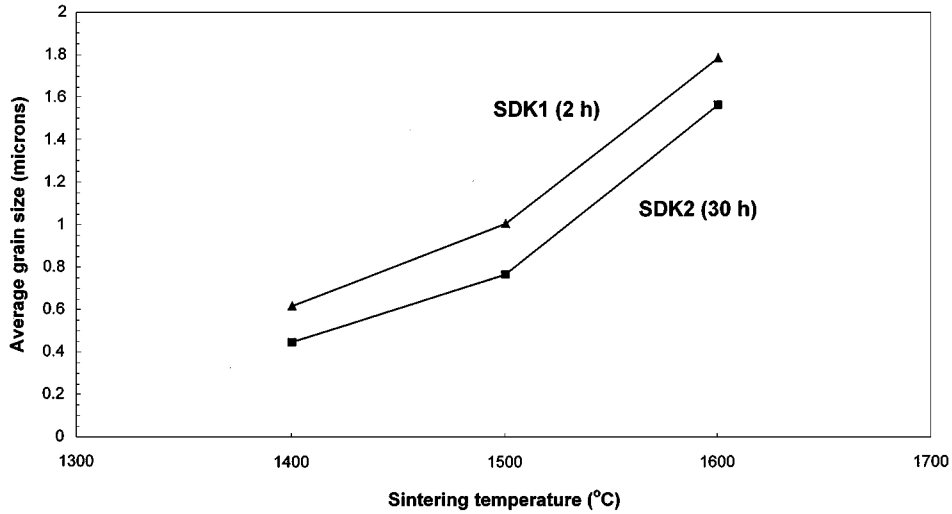

Figure 9 Influence of the dwell sintering temperature on the average grain size of 1 mm rods.

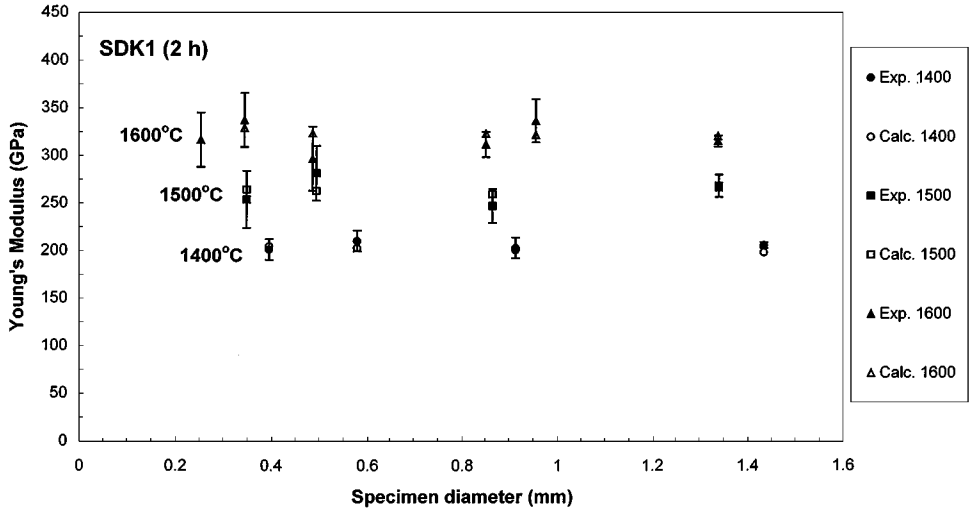

Figure 10 Comparison between experimental ("Exp.") and calculated ("Calc.") Young's moduli for SDK1 (2 h).

Young's modulus of fine-grained polycrystalline alumina and determined the following values for E_0 and b: $E_0 = 410.2$ GPa (± 3.5) and $b = 3.95$ (± 0.06). Hence Equation 3 now becomes:

$$E \text{ (in GPa)} = 410.2\, e^{-3.95P} \tag{4}$$

Density results (Figs 4 and 5) were therefore used to calculate the Young's modulus using Equation 4. Results are given in Figs 10 and 11, and show a good agreement between the experimental and the theoretical results. The comparisons between the fitted experimental and calculated values are listed in Table V. The maximum deviation was estimated at approximately 3% and proved the validity of Equation 4, for porosities up to 30%.

4.2. Calculation of flaw sizes

Considering the Griffith equation (1), the simplest situation is a crack extending through the thickness of a specimen and of length $2c$. The geometrical factor (Y) is then equal to $\sqrt{\pi}$, and the fracture mechanics equation becomes [19]:

$$\sigma_f = \frac{K_{IC}}{\sqrt{\pi c}} \tag{5}$$

Using $K_{IC} = 4$ MPa·m$^{1/2}$ for alumina, the flaw size can then be calculated by the following equation:

$$c \text{ (in microns)} \approx \frac{5.093.10^6}{\sigma_f^2} \tag{6}$$

where σ_f is the tensile strength in MPa.

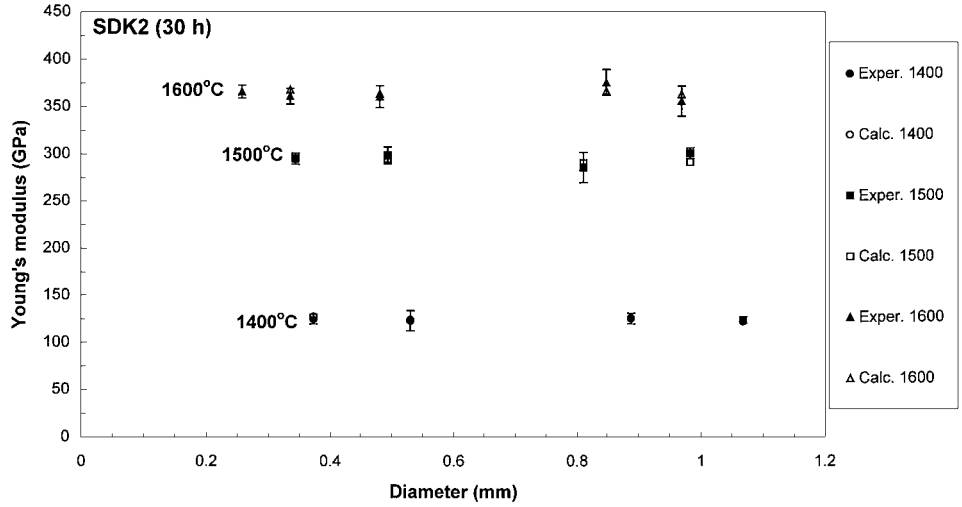

Figure 11 Comparison between experimental ("Exp.") and calculated ("Calc.") Young's moduli for SDK2 (30 h).

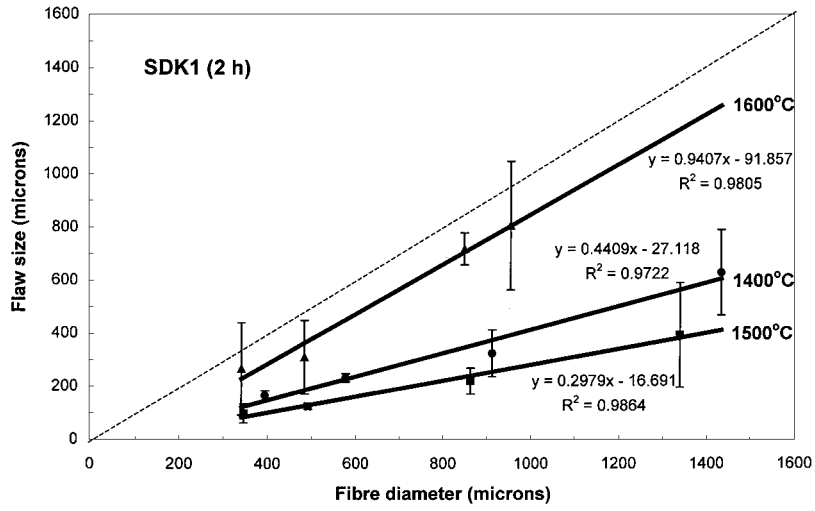

Figure 12 Flaw size, calculated using Equation 6, versus fibre diameter for SDK1 (2 h). The dotted line corresponds to the maximum flaw size, i.e. the fibre diameter.

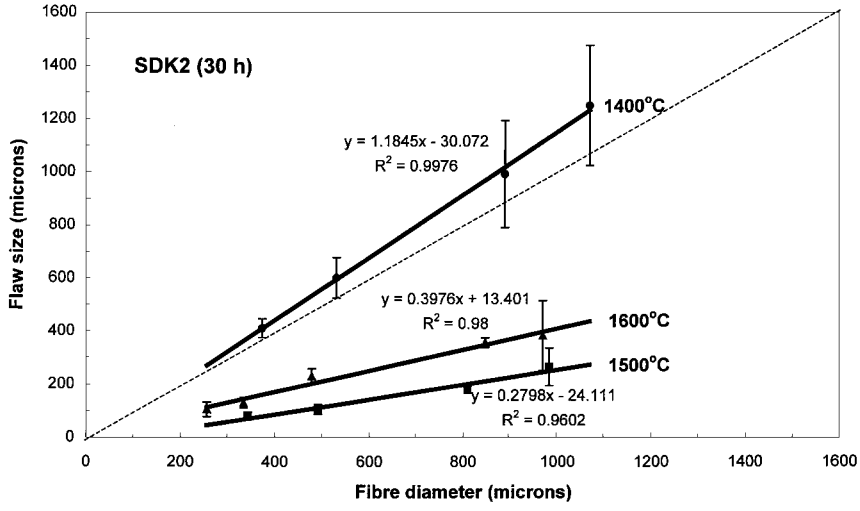

Figure 13 Flaw size, calculated using Equation 6, versus fibre diameter for SDK2 (30 h). The dotted line corresponds to the maximum flaw size, i.e. the fibre diameter.

For porosity levels below 20%, the calculated flaw sizes plotted against fibre diameters could be reasonably approximated by straight lines (Figs 12 and 13). This quantified the assumption used in the previous section to explain why strength decreased with fibre diameter, as it is more probable to find bigger strength-limiting defects in greater volumes. The gradient of the trendline was significantly higher for SDK1 (2 h), compared to SDK2 (30 h), at 1600°C. This confirms that less strength-limiting defects are created in a well-dispersed

Figure 14 Fracture view of a SDK1 (2 h) 1 mm rod (sintered at 1600°C) showing a crack extended through the thickness.

powder (SDK2 (30 h)) at high temperatures. A crack extended through the thickness of a SDK1 (2 h) 1 mm rod, sintered at 1500°C, is shown in Fig. 14. The size of this flaw, measured at 800 μm, approximately, using the SEM picture, could be estimated by considering the appropriate experimental fitting equation (given in Fig. 12). A value of 850 μm was calculated and, due to the approximations made to establish Equation 6 (fracture toughness, geometrical factor, etc), the agreement was considered relatively good.

The results also showed that Equation 6 could not be used for high porosity levels, as all maximum flaw sizes calculated for SDK2 (30 h) at 1400°C ($P \approx 30\%$) were larger than the corresponding fibre diameters. The flaw size was, however, relatively large for SDK2 (30 h) fibres and improvements have to be made to reduce it and, therefore, achieve better strengths.

5. Conclusions

The video extensometer successfully determined the mechanical properties of alumina fibres and rods made by colloidal processing. The results showed that the Young's modulus is a material property and is not size dependent, whilst any variation can be explained by the fibre porosity. The experimental data could be successfully fitted using Knudsen's simple empirical equation. The strength of the fibres increased with decreasing fibre diameter, as expected from the Griffith equation, because the size of the flaws was reduced. Again aggregates present in the fibres reduced the strengths by creating flaws, such as cracks and pores, during the sintering process. Exaggerated grain growth caused lower strengths at 1600°C. The maximum strengths were obtained for a dwell sintering temperature of 1500°C.

Better mechanical properties, i.e. higher Young's modulus and tensile strength, were achieved through controlled colloidal processing, by removing hard aggregates in particular. However, improvements have still to be made to limit the flaw size in the sintered body.

Acknowledgement

The main author would like to thank the European Union for funding under the Marie Curie Fellowship Number BRMA.CT98.5112.

References

1. I. A. AKSAY, *Adv. Cer.* **9** (1984) 94.
2. N. MCN. ALFORD, J. D. BIRCHALL and K. KENDALL, *Nature* **330** (1987) 51.
3. E. CARLSTRÖM, in "Surface and Colloid Chemistry in Advanced Ceramics Processing," edited by R. J. Pugh and L. Bergström (Marcel Dekker, New York, 1994) p. 1.
4. A. A. GRIFFITH, *Philos. Trans. R. Soc. Lond.* **A221** (1920) 163.
5. F. F. LANGE, *J. Am. Cer. Soc.* **72** (1989) 3.
6. R. J. HUNTER, in "Foundations of Colloid Science Vol. I" (Oxford University Press, New York, 1987).
7. C. GALASSI, E. RONCARI, R. GREENWOOD and A. PIANCASTELLI, *Key Eng. Mater.* **132–136** (1997) 329.
8. R. GREENWOOD and L. BERGSTRÖM, *J. Eur. Cer. Soc.* **17** (1997) 537.
9. D. COIMBRA, R. GREENWOOD and K. KENDALL, submitted.

10. J. B. WACHTMAN, "Mechanical Properties of Ceramics" (Wiley & Sons, New York, 1996).
11. R. W. RICE, *J. Mater. Sci.* **32** (1997) 3071.
12. R. GREENWOOD and K. KENDALL, in World Congress on Particle Technology (IchemE, Rugby, 1998) Paper 5, (CD-Rom).
13. O. BELLON, Ph.D. Thesis, Keele University, to be published, 1999.
14. R. MORRELL, in "Handbook of Properties of Technical & Engineering Ceramics, Part 1: An introduction for the engineer and designer," edited by National Physical Laboratory (Her Majesty's Stationery Office, London, 1985) Ch. 2.5.
15. *Idem*., in "Handbook of Properties of Technical & Engineering Ceramics, Part 2: Data Reviews, Section I—High-alumina ceramics," edited by National Physical Laboratory (Her Majesty's Stationery Office, London, 1987) p. 21.
16. J. D. BIRCHALL, in "Concise Encyclopedia of Composite Materials," edited by A. Kelly (Pergamon Press, Oxford, 1989) p. 215.
17. R. M. SPRIGGS, *J. Am. Cer. Soc.* **44** (1961) 628.
18. F. P. KNUDSEN, *ibid.* **45** (1962) 94.
19. A. DE S. JAYATILAKA, "Fracture of Engineering Brittle Materials" (Applied Science Publishers, London, 1979).

Received 23 April
and accepted 10 December 1999